



PCCP

**Structural and Energetic Properties of OC–BX₃ complexes:
Unrealized Potential for Bond-Stretch Isomerism**

Journal:	<i>Physical Chemistry Chemical Physics</i>
Manuscript ID	CP-ART-05-2021-002230.R1
Article Type:	Paper
Date Submitted by the Author:	25-Jun-2021
Complete List of Authors:	Munos, Jordan; University of Wisconsin - Eau Claire, Chemistry and Biochemistry Lowney, Diego; University of Wisconsin - Eau Claire, Chemistry and Biochemistry Phillips, James; University of Wisconsin - Eau Claire, Chemistry and Biochemistry

SCHOLARONE™
Manuscripts

Structural and Energetic Properties of OC–BX₃ Complexes: Unrealized Potential for Bond-Stretch Isomerism

Jordan A. Munos, Diego T. Lowney, and James A. Phillips*

Department of Chemistry and Biochemistry, University of Wisconsin – Eau Claire
105 Garfield Ave. Eau Claire, WI 45702

* Corresponding Author: phillija@uwec.edu; 715-836-5399

Abstract

We have explored the structural and energetic properties of OC–BX₃ (X = F, Cl, or Br) complexes using computations and low-temperature infrared spectroscopy. Quantum-chemical calculations have provided equilibrium structures, binding energies, vibrational frequencies, and B–C potential energy curves. The OC–BF₃ system is a weak, long-bonded complex with a single minimum on the B–C potential ($R(\text{B–C}) = 2.865 \text{ \AA}$). For the remaining two complexes, OC–BCl₃ and OC–BBr₃, computations predict two stable minima on their B–C potential curves. The BCl₃ system is a weak complex with a long bond ($R(\text{B–C}) = 3.358 \text{ \AA}$), but it exhibits a secondary, meta-stable minimum with a short bond length of 1.659 \AA . For OC–BBr₃, the system is a weak complex with a relatively short bond of 1.604 \AA (according to wB97X-D/aug-cc-pVTZ), but also has a secondary minimum at $R(\text{B–C}) = 3.483 \text{ \AA}$. This long-bond structure is the global minimum according to CCSD/aug-cc-pVTZ. In addition, the long-bond forms of both OC–BCl₃ and OC–BBr₃ were observed in matrix-isolation IR experiments. The measured CO stretching frequencies were 2145 cm^{-1} and 2143 cm^{-1} , respectively. No signals due to the short-bond forms of OC–BCl₃ and OC–BBr₃ were observed.

Introduction

Interest in molecular complexes and their structural and energetic properties has continued for years since the 1960's (1, 2). One reason for this continued interest stems from on-going computational chemistry research. From a practical standpoint, developers of various density functional theory (DFT) methods such as M06 and M06-2X (3, 4) have used the "Charge Transfer Database" (in part) to validate energy results. Computational investigations have also provided a great deal of insight into the complex and often ambiguous the bonding interactions in these systems, which has been illustrated in a few comprehensive, comparative studies (5, 6). These efforts identified a continuous range of interactions that spans from van der Waals interactions to covalent bonds, and moreover, they found that no one feature (e.g., electrostatics, charge-transfer, etc.) contributed a fixed amount the binding energy, or paralleled strength in any consistent, systematic manner. In addition, computations have led to a more systematic classification that makes reference to the geometries about the electron deficient regions of the acceptor center. These are known as " σ -hole" and " π -hole" interactions (7-9). Common examples of σ -hole interactions include hydrogen bonding (7, 8), halogen bonding (7, 8), and MX_4 coordinate bonds (9). The most common examples of π -holes are in Group 13 (MX_3) acceptors such as BCl_3 (10).

Another reason for the on-going interest in these systems is that some molecular complexes undergo major changes in structure when going from the gas phase to the solid state or other stabilizing, condensed-phase environment. Perhaps the most vivid examples are the nitrile- BF_3 complexes (11, 12) - π -hole complexes - for which there are documented structural changes across a range of environments. The specific signature of this effect is a contraction of the B-N

distance and a distortion of the acceptor molecule (BF_3), and the clearest illustrations are gas-solid structure differences. For example, the gas-phase structure of $\text{CH}_3\text{CN}-\text{BF}_3$ has a B-N distance of 2.011 Å (13), but the donor-acceptor bond contracts by 0.381 Å in the solid state, to a distance of 1.630 Å (12, 14). In the case of $\text{HCN}-\text{BF}_3$ (15), $\text{FCH}_2\text{CN}-\text{BF}_3$ (16), and $\text{ClCH}_2\text{CN}-\text{BF}_3$ (16), the effect is even more extreme with B-N distances contracting by 0.7 Å to 0.8 Å between the gas phase and the solid state.

For the nitrile- BF_3 systems, significant changes in structure can even be induced by inert media such as noble gas matrices, and this sensitivity stems from an extreme anharmonicity in the donor-acceptor potential (11). The experimental signature of this effect is a shift in a key acceptor mode in the infrared (IR) spectra of the complexes (relative to the free acceptor), which has been shown to parallel the B-N distance, and thus reflects a progressive contraction of the B-N bond (17). Scans of the donor-acceptor potential have identified a distinct shape in these medium-sensitive systems, characterized by a long equilibrium distance and a gentle rise toward the inner wall of the curve (18, 19). The generalized mechanism for condensed-phase structural change is as follows; in dielectric media, the inner region is preferentially stabilized, such that the minimum shifts inwards via solvent interactions. Models based on this effect reproduce the observed, ~ 0.7 Å contraction in the B-N bond for $\text{FCH}_2\text{CN}-\text{BF}_3$ (18). In an extreme case, similar models predict a 1.0 Å shortening for $\text{CH}_3\text{CN}-\text{SiF}_4$ (19), from 3.0 Å in the gas phase to 2.0 Å in a dielectric media of with $\epsilon = 20$.

In subsequent studies of the BCl_3 analogs of these nitrile- BF_3 systems (20, 21), a different, novel aspect of the intermolecular potential was discovered – the occurrence of two distinct minima along the B-N coordinate. These minima, corresponding to so called “short-” and “long-bond” structures, is reminiscent of a phenomenon known as “bond-stretch isomerism,” which has been a contentious topic since the 1990’s (22, 23). To some extent, the idea of bond-stretch isomers had been dismissed due to the lack of experimental evidence, yet theoretical predictions of such systems continue to arise (24-26). Nonetheless, computational results for $\text{CH}_3\text{CN-BCl}_3$ predicted two distinct minima at 1.601 Å and 2.687 Å (20) separated by a significant barrier, which persisted at high-levels of theory (CCSD/aug-cc-pVTZ). However, only signals due to the short-bond form were observed in matrix-isolation IR experiments, in part because overlapping signals in the nitrile stretching region impeded assignment of peaks due to the long-bond structure.

Similar results were obtained when this work was extended to $\text{FCH}_2\text{CN-BCl}_3$ and $\text{ClCH}_2\text{CN-BCl}_3$ (21). In the case of $\text{CH}_3\text{CN-BCl}_3$, the short-bond form was much lower in energy, but for $\text{FCH}_2\text{CN-BCl}_3$ and $\text{ClCH}_2\text{CN-BCl}_3$ (21), the addition of halogens weakened the bond, rendering the two minima much closer in energy. The binding energies (global minima) for the short-bond forms were 5.3 kcal/mol and 6.3 kcal/mol for $\text{FCH}_2\text{CN-BCl}_3$ and $\text{ClCH}_2\text{CN-BCl}_3$, respectively. Notably, the energy of the long-bond forms (3.2 kcal/mol and 3.3 kcal/mol) were much less affected by halogen substitution, and were nearly equal to the for $\text{CH}_3\text{CN-BCl}_3$. However, in spite of the fact that halogen substitution did equalize the energies of the two minima to some extent, only signals for the short-bond form were observed in matrix-IR experiments.

Here, we extend this work to similar systems for which there are some other advantageous features. Carbon monoxide (CO) is isovalent with nitriles, but is a much simpler donor with only one vibrational frequency in a sparse region of the spectrum, which would minimize overlap with other signals, and presumably facilitate the observation of distinct, but often slight, frequency shifts. In addition, we explore a wider range of halogens on the BX_3 acceptors. This manuscript will report the structural and energetic properties of $OC-BX_3$ ($X = F, Cl$ or Br) complexes, including equilibrium structures, predicted gas-phase frequencies, and potential energy curves, via quantum-chemical computations and IR experiments in Ar and Ne matrices. The BCl_3 and BBr_3 complexes with CO both show potential for the observation of distinct structures with different B-C minima, particularly in the latter case. By contrast, $OC-BF_3$ is a weakly-bonded system with a known experimental structure (27), which did provide a valuable computational benchmark.

Materials and Methodology

Computations

Post Hartree-Fock and DFT calculations were performed using Gaussian09 B.01 (28) and Gaussian16 C.01 (29). Symmetry was constrained to C_{3v} geometry throughout these computational studies. Optimizations were performed with convergence criteria set using the “opt=tight” option, and an ultrafine grid was employed for all DFT and MP2 calculations.

Overall, we utilized multiple DFT methods (M05 (30), M06 (3), M06-2X (3), ω B97X-D (31), M08-HX (32), M11(33), MN12-SX (34), and MN15 (34)) along with MP2 (35) and CCSD (35)

with the aug-cc-pVTZ basis set (35). A validation study was conducted, as in previous work by the group, which was based on acceptor frequencies and experimental gas-phase structures (16, 20). The structures and binding energies reported here are from ω B97X-D, which had the smallest RMS error when predicting experimental BF_3 and BCl_3 frequencies (7.23 cm^{-1} and 8.75 cm^{-1} for BF_3 and BCl_3 , respectively) (36). In addition, ω B97X-D also most accurately predicted the experimental structure of OC-BF_3 (0.023 \AA difference in the B-C distance) (27). However, we do note that M06 was somewhat more accurate in predicting BBr_3 frequencies ($\text{RMS}_{\text{M06}} = 3.2 \text{ cm}^{-1}$ and $\text{RMS}_{\omega\text{B97X-D}} = 13.5 \text{ cm}^{-1}$). We note here that none of these methods explored were particularly effective in predicting the frequency of free CO (within 30 cm^{-1}). In the end we observed only peaks in the CO region, and thus utilized predicted shifts (as opposed to absolute frequency values) to assist in our peak assignments.

The B-C potential was mapped in a pointwise manner from 1.4 \AA to 3.0 \AA in steps of 0.1 \AA using the following methods: M05, M06, M06-2X, ω B97X-D, MP2, and CCSD, all with the aug-cc-pVTZ basis set. The energies on the CCSD curves were based on MP2 geometries. Among these methods, ω B97X-D most closely matched the CCSD energies along these curves, but most methods—aside from MP2—were qualitatively similar. The notable exception is that the CCSD energies identify a different global minimum in the case of OC-BBr_3 (see below), but the overall energy difference is slight.

Materials

CO (99.0%) was obtained from Sigma-Aldrich and used without further purification. BCl₃ (99.9%) was obtained from Sigma-Aldrich and was transferred to a sample tube by filling a 2L bulb to a pressure of 1-2 atm, and then condensed in a 50mL sample tube with liquid nitrogen. Both BCl₃ and BBr₃ are highly corrosive substances which readily react with trace amounts of water to produce HCl and HBr, respectively. Further purification of the BCl₃ sample was necessary to remove a persistent HCl impurity, and was achieved through a two-step process: first freeze-pump-thaw cycles at the temperature of liquid nitrogen (77K), then the sample was subjected to active vacuum in several 10-30 second intervals at 183K via a liquid nitrogen/methanol bath. BBr₃ was obtained at a purity of 99.995% from Sigma-Aldrich, and was transferred to a sample tube via a disposable pipet, and prior to use was further purified by freeze-pump-thaw cycles in a liquid nitrogen bath at 77K. Ar (99.9999%) and Ne (99.999%) were obtained from Praxair and used with no further purification.

Matrix-Isolation IR Spectra

IR spectra were collected using two previously described matrix-isolation apparatuses. Initial spectra in argon matrices were collected using a ~10K system (37, 38) that utilizes a Cryomech ST15 optical cryostat and a Nicolet Avatar iS20 FTIR spectrometer at 1.0 cm⁻¹, averaging 400 scans per spectrum. Matrix samples were deposited on a KBr window, and the temperature was maintained using a Scientific Instruments 9600-1 temperature controller with a single Si diode located at the end of the second refrigeration stage. The majority of experiments were conducted in neon matrices on a 4K system (20, 39) that employs a Janis SHI-4-5 optical cryostat and a

Thermo Nexus 670 FTIR. The resolution was 1.0 cm^{-1} , and 400 scans were averaged for each spectrum. Matrix samples were deposited onto a gold mirror and spectra were collected by reflecting the IR beam off the sample mirror ($\sim 45^\circ$) and onto an external (DTGS) detector. Samples were prepared in 2L glass bulbs on a glass manifold (Chemglass) evacuated with a diffusion pump (Chemglass) by making separate gas mixtures containing either CO or BX_3 ($X = \text{Cl}$ or Br) in Ar or Ne. For experiments, matrix samples were deposited by simultaneous flow of gas mixtures in separate lines that merge immediately before the mirror. A final set of experiments using single mixtures containing both guest gases in the same bulb and deposition line yielded identical spectra. Mixtures were deposited at temperatures ranging from 3.5K to 6K and in most experiments we ran two to four 60-minute depositions, after which most samples were annealed at temperatures of 8-9K for 30 minutes to one hour with spectra recorded after each deposition and anneal. Flow rates typically ranged from 1 to 10 mmol/hr with mixture concentrations ranging from 1/32%-1/2%. It should be noted that faster deposition rates seemed to reduce the amount of HX in the spectra, relative to BX_3 . This suggests decomposition in the deposition plumbing, in spite of the fact that the lines were mainly Teflon, with as little metal plumbing as possible in an effort to minimize this outcome (20).

Bulk Reactivity

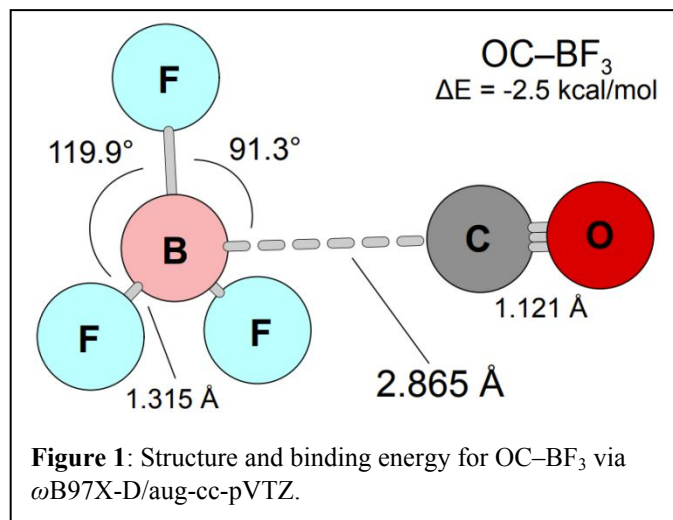
To ensure that we could perform the single-bulb experiments described above, we examined the direct reaction of CO and BCl_3 or BBr_3 . In this experiment, ~ 50 torr each of BBr_3 and CO were introduced into a 100mL reaction flask on our preparatory manifold. The gases were allowed to mix for ~ 20 minutes before sitting in an ice bath for ~ 10 minutes. Neither measure produced a visible reaction product.

Results and Discussion

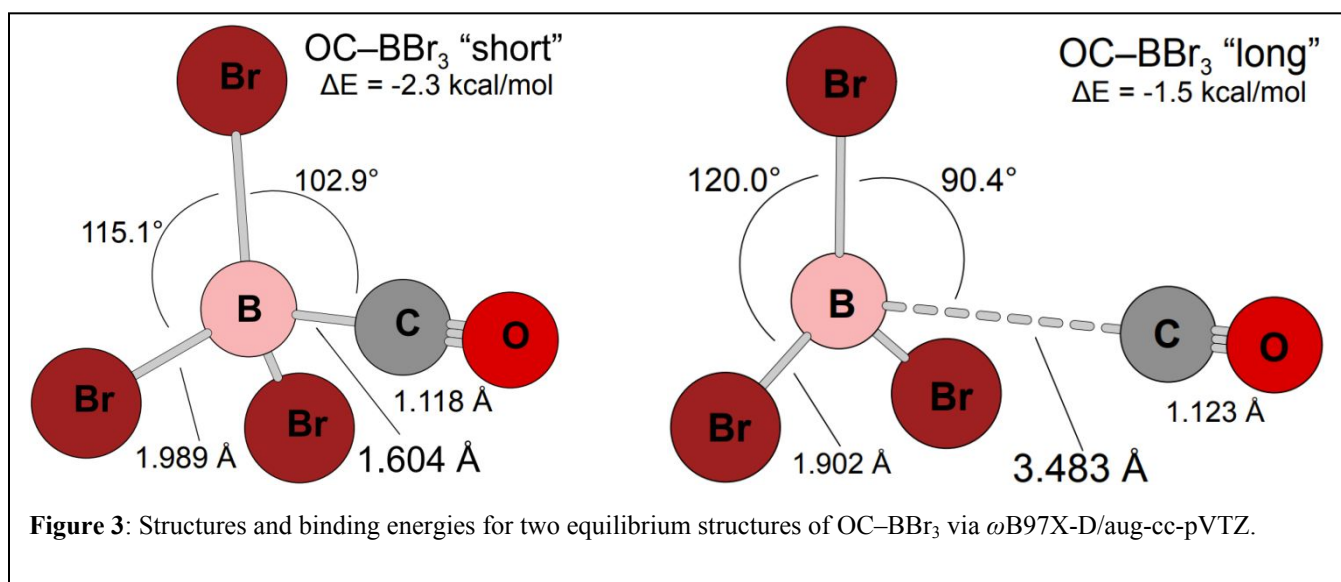
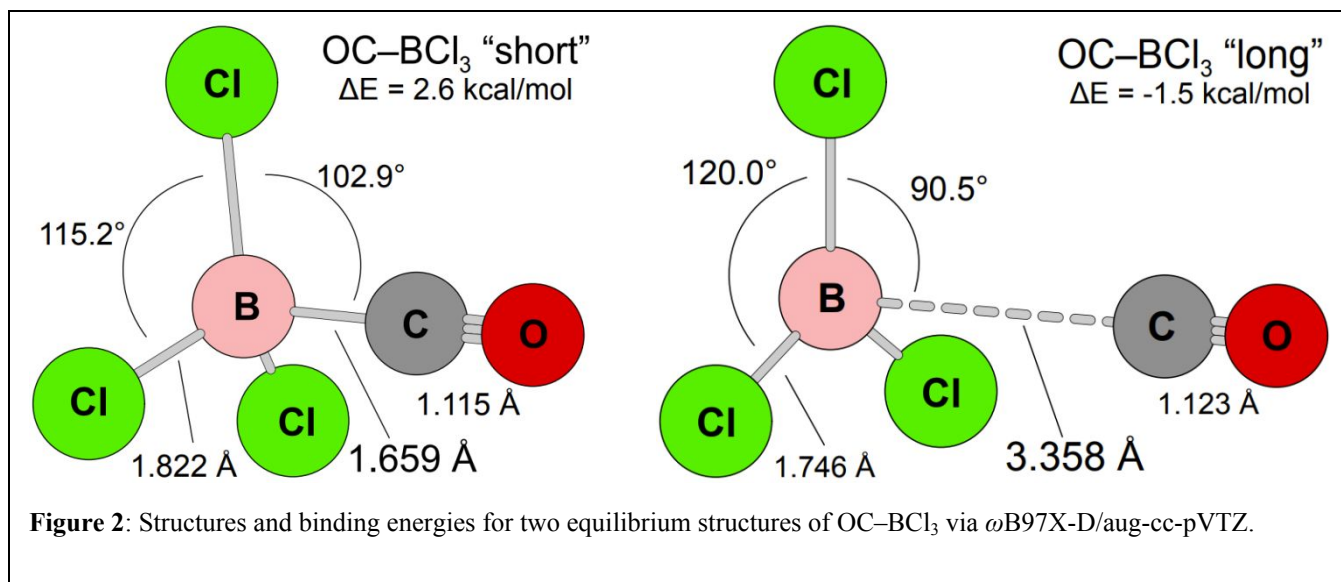
Equilibrium Structures

Due to previous work on $\text{CH}_3\text{CN}-\text{BCl}_3$ (20) and $\text{XCH}_2\text{CN}-\text{BCl}_3$ (21), we expected two distinct structures with different B-C distances for $\text{OC}-\text{BCl}_3$ and $\text{OC}-\text{BBr}_3$. Thus, when searching for equilibrium structures we started the optimizations from two different geometries with short (1.6 Å) and long (3.0 Å) B-C distances. As noted above, we used a variety of DFT methods as well as MP2 and CCSD, settling on $\omega\text{B97X-D}$ for most of the structure and binding energy results reported in this manuscript. All other methods produced relatively consistent results.

All structural parameters for $\text{OC}-\text{BF}_3$ are shown in Figure 1. This complex is a weakly-bonded system and has a single, distinct structure with a long B-C distance (2.865 Å) and a binding energy of 2.5 kcal/mol. These results are consistent with the recently-updated structure of $\text{OC}-\text{BF}_3$ (27), which puts the B-C distance at 2.888 Å. For context, the van der Waals radii (40) for carbon (1.7 Å) and boron (1.8 Å) add to a sum of 3.5 Å, 0.6 Å longer than the B-C distance of $\text{OC}-\text{BF}_3$, while the sum of the covalent radii (41) for carbon (0.77 Å) and boron (0.84 Å) is 1.61 Å, significantly shorter than the calculated B-C distance of 2.865 Å. The acceptor molecule (BF_3) has little distortion from its trigonal-planar geometry; the F-B-C angle is 91.3°. Compared to $\text{HCN}-\text{BF}_3$, a similar, isoelectronic complex (5, 42), $\text{OC}-\text{BF}_3$ has a considerably longer donor-acceptor distance. For $\text{HCN}-\text{BF}_3$, the experimental B-N distance is 2.473 Å (5, 42), almost an angstrom shorter than the van der Waals radii. The binding energy of the HCN complex is 5.0 kcal/mol via $\omega\text{B97X-D}/\text{aug-cc-pVTZ}$ (present work), which makes the complex twice as strong as the analogous CO complex, which has a binding energy of 2.5 kcal/mol.



By contrast, we predict two structures for the OC-BCl₃ and OC-BBr₃ complexes, which we refer to as the “short-” and “long-bond” forms henceforth. The long-bond forms of OC-BCl₃ and OC-BBr₃ are generally similar to the OC-BF₃ complex; all are weakly-bonded structures with little distortion in the acceptor subunit. Both have slightly longer B-C distances than the BF₃ complex, 3.358 Å and 3.485 Å, respectively, much closer to the sum of the carbon and boron van der Waals radii. Both complexes exhibit similar X-B-X and X-B-C angles with the former being 120°, and the latter being 90.5° and 90.4° respectively, indicating slightly less distortion than in OC-BF₃. A complete set of structural parameters are included in Figures 2 and 3. Binding energies for the Cl- and Br-containing complexes are both 1.5 kcal/mol, which are 1.0 kcal/mol smaller in magnitude than the analogous BF₃ complex.



These long-bond structures resemble their analogs in the nitrile- BCl_3 systems (e.g., $\text{CH}_3\text{CN-BCl}_3$) (20). Again, while the donor-acceptor distances cannot be directly compared due to differences in the atoms of the interaction, an indirect comparison can be based on van der Waals radii. For $\text{CH}_3\text{CN-BCl}_3$, the predicted MP2/aug-cc-pVTZ B-N distance is 2.687 Å, 0.663 Å shorter than the sum of the van der Waals radii, while the B-C distances for the OC-BCl_3 and

OC–BBr₃ forms differ by only 0.142 Å and 0.015 Å respectively. This points to a slightly weaker interaction in the long-bond forms of the OC–BX₃ complexes, compared to CH₃CN–BCl₃. This observation is substantiated by the values of the binding energies; which are 1.5 kcal/mol for both complexes. By contrast, CH₃CN–BCl₃ ($\Delta E = -4.9$) is more strongly bound than the CO complexes by almost 3.5 kcal/mol. Overall, both long-bond forms of OC–BCl₃ and OC–BBr₃ are fairly weak complexes, with little distortion in the acceptor molecule, and long donor-acceptor distances approaching the sum of their respective van der Waals interaction radii.

Turning now to the short-bond structures for both the Cl- and Br-complexes, we found both systems exhibit large distortions of the acceptor molecule due to the short B-C distances. For OC–BCl₃, the B-C distance is 1.659 Å, which is 0.055 Å longer than OC–BBr₃ ($R(\text{B-C}) = 1.604$ Å). The X-B-C angles are both 102.9°. In these structures, both B-C distances are close to the sum of the covalent radii of boron (0.84 Å) and carbon (0.77 Å) which is 1.61 Å, an indication that the interactions in these short-bond forms involve some degree of charge transfer and/or covalent bonding. In contrast to their long-bond counterparts, the binding energies of these structures, are not similar. For OC–BCl₃, the energy lies above that of the separated fragments ($\Delta E = +2.5$ kcal/mol), while for OC–BBr₃ the overall energy lies 0.8 kcal/mol below its long-bond counterpart ($\Delta E = -2.3$ kcal/mol). However, we note that the CCSD/aug-cc-pVTZ energies, as inferred from the B-C potential scans (see below), indicate that the long-bond form is actually the global energy minimum. As a whole, the situation with these systems resembles that for the N₂–BH₃ complex (43), in which the B-N distance is quite short, but the binding energy is small; the bonding interactions are offset by significant repulsive interactions between donor and acceptor.

Structurally, these short-bond forms resemble the analogous short-bond structure for the $\text{CH}_3\text{CN}-\text{BCl}_3$ system (20). The B-N distance is 1.601 Å, a bit longer than the sum of the covalent radii, by 0.051 Å. The $\text{OC}-\text{BCl}_3$ complex has a donor-acceptor distance that is also just longer than the sum of the covalent radii (0.049 Å), while for $\text{OC}-\text{BBr}_3$ the value is 0.006 Å shorter than that predicted by covalent radii. The distortion of the Cl-B-N angle in the short-bond $\text{CH}_3\text{CN}-\text{BCl}_3$ is almost 2° larger than the analogous angle in the $\text{OC}-\text{BX}_3$ complexes, and the binding energy of the nitrile complex is larger. These indicate a stronger interaction for $\text{CH}_3\text{CN}-\text{BCl}_3$, relative to the short-bond $\text{OC}-\text{BX}_3$ structures, but they are qualitatively similar nonetheless.

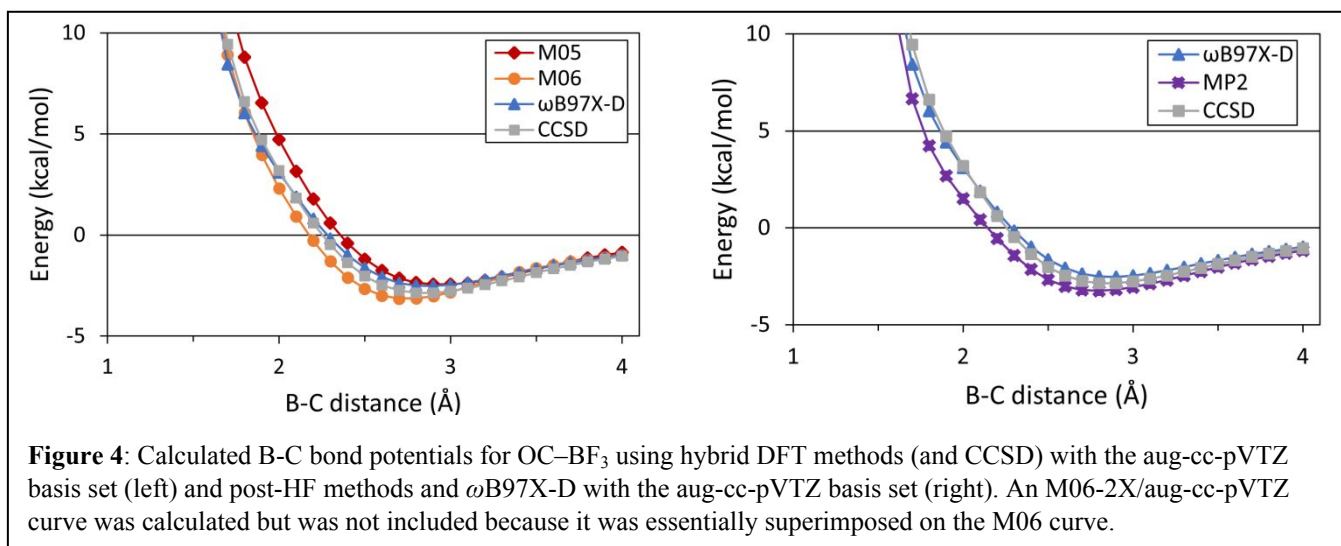
For a more classic example, we turn to $\text{H}_3\text{N}-\text{BCl}_3$ (5, 44). Here the B-N distance is 1.618 Å, again just longer (0.068 Å) than the sum of the covalent radii. However, the binding energy for the ammonia complex is significantly larger in magnitude than those of the CO complexes; 28.2 kcal/mol (via MP2/6-31+G(2d,p)//MP2/6-31+G(2d,p)) (44). Compared to the short-bond form of $\text{CH}_3\text{CN}-\text{BCl}_3$, the ammonia complex has a longer bond, but stronger interaction. An analogous trend had been noted previously in $\text{RCN}-\text{BH}_3$ complexes (45), which have shorter B-N bonds and a smaller $|\Delta E|$ compared their amine counterparts. The difference is that ammonia has an sp^3 -like lone pair, which is more extended in space than the sp -like lone pair of the nitriles, allowing for overlap to occur at a longer distance. By contrast, the sp -like lone pair of the CH_3CN extends to a lesser degree, and must be closer to the acceptor molecule for significant overlap to occur. At these short distances, the π electrons of the C-N triple bond and the halogens of the acceptor molecule repel each other significantly, which (as noted above for N_2-BH_3)

raises the overall energy, offsetting the energetically-favorable bonding interactions. The end result is an interaction that is shorter and weaker for the CH_3CN complex than for $\text{NH}_3\text{-BH}_3$. In the present case, OC-BCl_3 and OC-BBr_3 are structurally indicative of significant covalent or charge-transfer interactions, with short donor-acceptor distances close to the sum of their covalent radii and large distortions of the acceptor molecules. However, from an energetic standpoint these complexes are fairly weak, and by analogy to the nitrile- BX_3 systems (11), we presume this also stems from the repulsive contribution to the energy at these inner distances.

Donor-Acceptor Potentials

Figures 4 through 6 display the boron-carbon potential energy curves computed via a variety of DFT methods along with MP2 and CCSD and the aug-cc-pVTZ basis set. These curves offer two major observations; one being the relative energy between the two minima of the Cl- and Br-containing complexes, the other being the barrier that exists between these two distinct minimum-energy structures. For OC-BF_3 , we note that the curve resembles those of systems prone to condensed phase media effects, with its relatively long minimum and gentle rise towards the inner portion of the curve (11). Interestingly, the system has been studied via matrix-IR (46, 47), and the measured frequencies nearly agree with our predictions, but there is the slightest indication of a matrix-induced contraction of the B-C bond. The B-F asymmetric stretching bands of OC-BF_3 had been previously observed at $1438.7/1437.3\text{ cm}^{-1}$ and 1441 cm^{-1} in argon matrices (46, 47). In this work, we predict a frequency at 1444 cm^{-1} ($\omega\text{B97X-D/aug-cc-pVTZ}$) for this band. This is in reasonable agreement, however, the $3\text{-}7\text{ cm}^{-1}$ red shift between the matrix data and the gas-phase predictions is consistent with a slight compression of the B-C bond (though the difference is arguably near the RMS error in our frequency predictions).

For OC–BCl₃, the energy maximum occurs around 2.1 Å (+5.9 kcal/mol) with the energy +7.4 kcal/mol relative to the outer minimum, and the two minima are 4.1 kcal/mol apart. For OC–BBr₃, the barrier occurs at 2.2 Å (+5.7 kcal/mol) with the energy +7.2 kcal/mol relative to the outer minimum. The two minima are closer in energy to each other than those of the BCl₃ complex with a difference of only 0.8 kcal/mol between them. It should be noted that CCSD predicts a significantly higher energy along the inner part of the curve (relative to all DFT methods), and indicates that the long-bond structure is the global energy minimum. Moreover, this result is more consistent with what we observe in our experiments (see below).



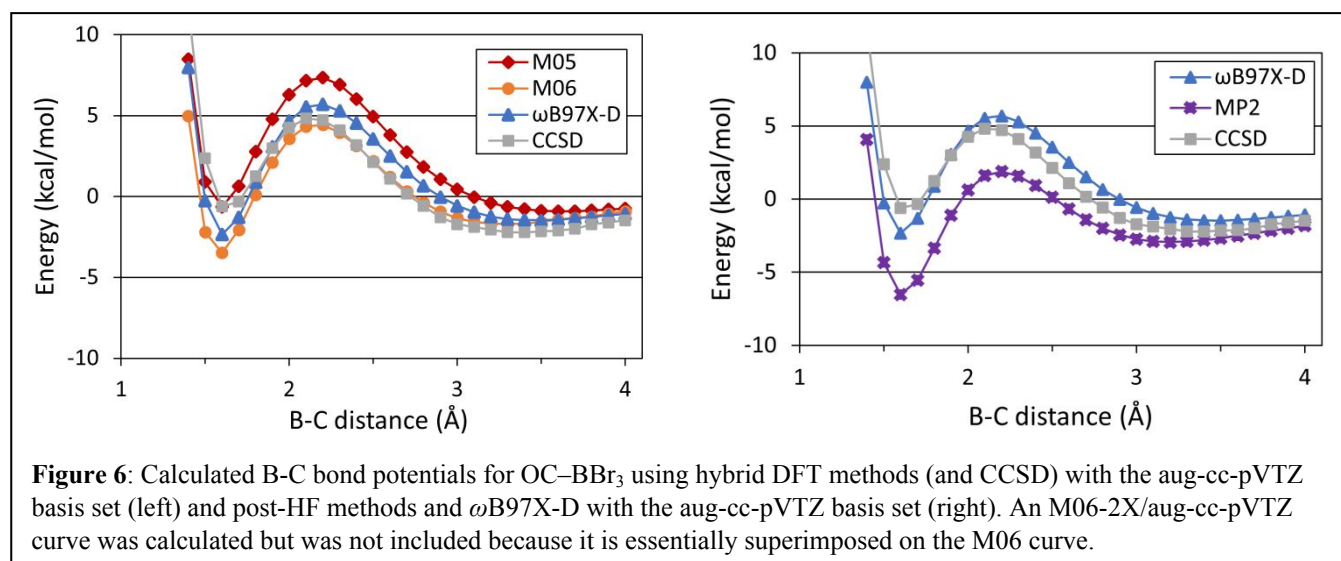
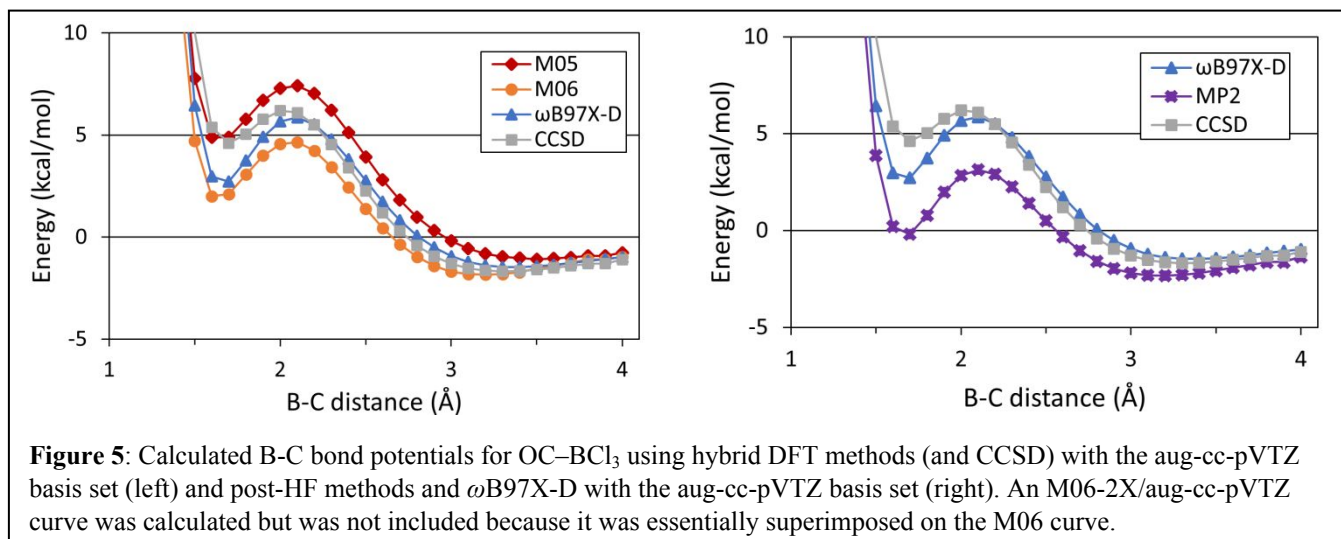


Figure 7 shows two different overlays for the three complexes, one for the ω B97X-D potentials and another for the CCSD potentials, to facilitate comparison between the shapes of the respective curves. The graphs not only display the clear difference in energy between the two

minima for the BCl_3 and BBr_3 complexes; but also, the difference in the calculated energies between DFT and CCSD. Again, for $\omega\text{B97X-D}$, the calculations predict a much lower-energy inner minimum for BBr_3 with a higher-energy outer minimum, while CCSD does the exact opposite. For the BF_3 complex, CCSD predicts a similar energy rise to that for $\omega\text{B97X-D}$, and the minimum energy points lie at nearly the same B-C distances, 2.9 Å and 2.8 Å for $\omega\text{B97X-D}$ and CCSD, respectively. Another observation these graphs lend themselves to is an explanation as to why BF_3 does not show a barrier, and in turn, two distinct structures like the BCl_3 and BBr_3 complexes. Overall, this situation mimics what we encountered previously for nitrile- BX_3 complexes (11), and rationalized via energy decomposition analyses (45). In the systems with the larger halogens (Cl, and presumably Br), the barrier results from repulsion between the halogens and the π electrons on C-N or C-O, which set in at fairly long distances. At shorter distances, these repulsions are offset by bonding interactions (more or less). This effect has been further illustrated in a study of the HCN-BCl_3 complex, by comparing the B-N potentials obtained both with and without relaxed fragment geometries(26). For BF_3 systems, the favorable bonding interactions and π -halogen repulsions set in at similar distances, rendering the potentials flat (and leading to medium effects for nitrile- BF_3 systems) (11).

Lastly, the overall trends in the energies in the short- and long-bond regions of the curve can be rationalized in terms of key acceptor properties (i.e., charge on the boron atom and LUMO energies). The energy in the short-bond region parallels LUMO energies ($\text{BBr}_3 < \text{BCl}_3 < \text{BF}_3$), which one might expect to correlate with stronger bonding interactions ($\text{BBr}_3 > \text{BCl}_3 > \text{BF}_3$). On the other hand, the charge on the central atom is greatest on BF_3 , and this seems consistent with

OC–BF₃ having the lowest energy minimum in the long bond region (though arguably this effect is convoluted with the barrier stemming from the onset of repulsions for BCl₃ and BBr₃).

Table 1: Summary of boron charges and LUMO energies

Acceptor molecule	q_B (e)	E_{LUMO} (eV)
BF ₃	+1.40	+0.044
BCl ₃	+0.34	+0.002
BBr ₃	+0.06	-0.013

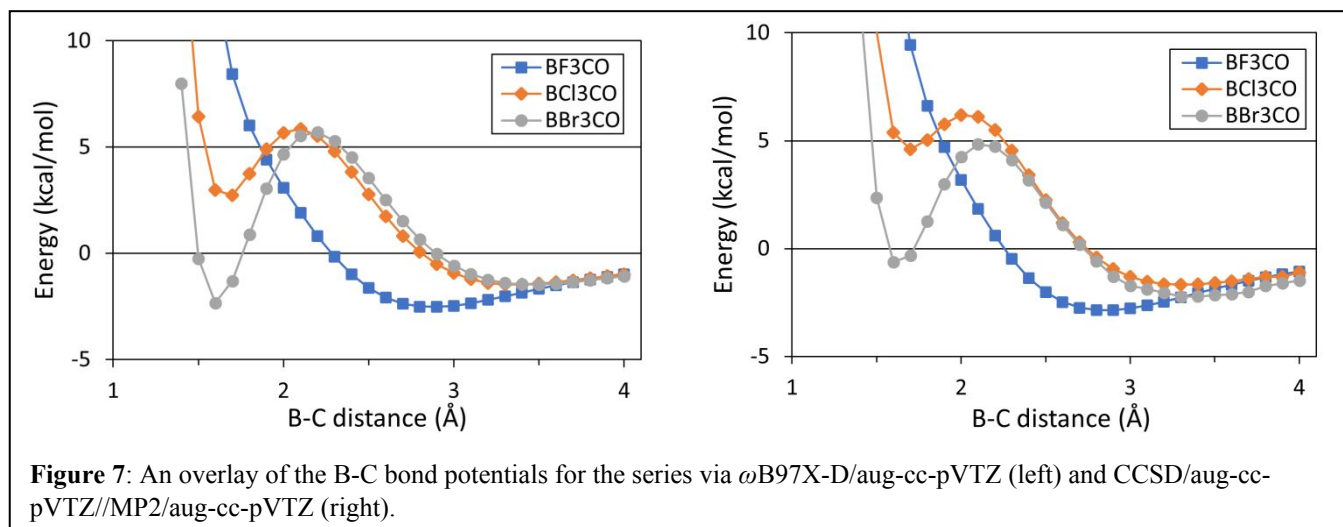


Figure 7: An overlay of the B-C bond potentials for the series via ω B97X-D/aug-cc-pVTZ (left) and CCSD/aug-cc-pVTZ//MP2/aug-cc-pVTZ (right).

IR Spectra and Frequencies

We recorded IR spectra of OC–BCl₃ and OC–BBr₃ in low-temperature matrices, focusing mainly on solid neon, although we did perform some CO/BCl₃ experiments in solid argon as well. For both OC–BCl₃ and OC–BBr₃, we were able to assign one band in the CO region to the 1:1 OC–BX₃ complex, and this guided by predicted frequency shifts (ω B97X-D/aug-cc-pVTZ). Figures 8 and 9 show, respectively, the spectra in the CO regions for both CO/BCl₃ and CO/BBr₃ experiments in solid neon. In the OC/BCl₃ data, we see two product peaks that do not appear in the CO (or BCl₃) reference spectra. Of these, we assigned the peak at 2144 cm⁻¹ to the long-bond form of the complex, while the peak at 2154 cm⁻¹ is due to OC–HCl arising from the persistent HCl impurity. As noted above, while specific frequency predictions agree only marginally with what is observed in experiments, calculated shifts (complex – free CO) are reasonably consistent with observations. For the short-bond form of OC–BCl₃, the CO stretching frequency is predicted to be at 2313 cm⁻¹ (shift of +73) and was not observed in the experiments. As for the long-bond form, predictions have a vibration at 2248 cm⁻¹ (+7). A peak at 2145 cm⁻¹ (+4) was assigned to the long-bond form. We predict CO stretching frequency of OC–HCl at 2261 cm⁻¹ (+20) and experimentally assigned it to a peak at 2154 cm⁻¹ (+13). Table 2 also includes product band assignments and peak shifts for argon experiments. Peaks were assigned in a similar fashion as described with the neon experiments.

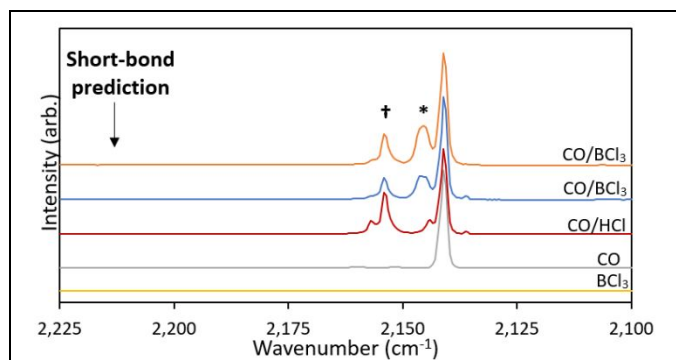


Figure 8: IR spectrum of OC–BCl₃ in solid Ne. Spectra as marked with the top trace reflecting 30 minutes of annealing at 9K. The assigned complex peak is marked with an asterisk (*) and the impurity (OC–HCl) peak is marked with a dagger (†). The expected position of the short-bond form of OC–BCl₃ is noted.

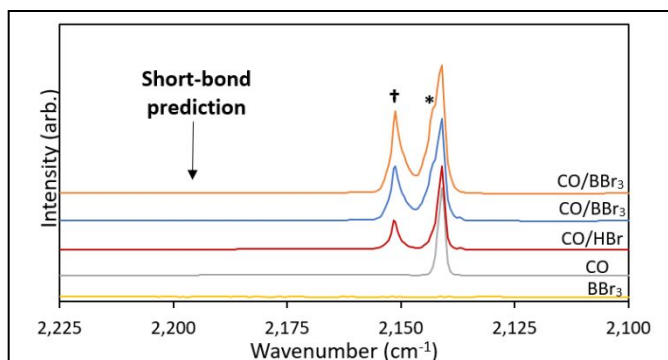


Figure 9: IR spectra of OC–BBr₃ in solid Ne. Spectra as marked with the top trace reflecting 30 minutes of annealing at 9K. The assigned complex peak is marked with an asterisk (*) and the impurity (OC–HBr) peak is marked with a dagger (†). The expected position of the short-bond form of OC–BBr₃ is noted.

Table 2: Observed and calculated vibrations frequencies of OC–BCl₃

	Frequency (cm ⁻¹)			Shifts (cm ⁻¹)		
	Obs. ^a (Ne)	Obs. ^a (Ar)	Calc. ^b	Obs. ^a (Ne)	Obs. ^a (Ar)	Calc. ^b
OC–BCl ₃ (long) ^c	2145	2143	2248	+4	+6	+7
OC–BCl ₃ (short) ^d	-	-	2313	-	-	+73
OC–HCl	2154	2153	2261	+13	+16	+20

a) Margin of error: ± 1 cm⁻¹. b) ω B97X-D/aug-cc-pVTZ. c) Bond length: 3.358 Å. d) Bond length: 1.659 Å.

Table 3 shows all peak assignments and shifts for the 1:1 OC–BBr₃ complex. In OC/BBr₃ experiments, we again observed two product peaks at 2143 and 2151 cm⁻¹. The CO stretch for long-bond form was predicted at 2246 cm⁻¹ (+5) and was observed at 2143 cm⁻¹ (+2), as a shoulder on the high-frequency edge of the free CO peak. The CO stretch for the OC–HBr complex predicted at 2244 cm⁻¹ (+3), and thus, we assign the peak at 2151 cm⁻¹ (+10) to OC–

HBr. The CO stretch of the short-bond form of OC–BBr₃ complex, calculated at 2230 cm⁻¹ (+56), was not observed.

Table 3: Observed and calculated vibrational frequencies of OC–BBr₃

	Frequency (cm ⁻¹)		Shifts (cm ⁻¹)	
	Obs. ^a (Ne)	Calc. ^b	Obs. ^a (Ne)	Calc. ^b
OC–BBr ₃ (long) ^b	2143	2246	+2	+5
OC–BBr ₃ (short) ^c	-	2230	-	+56
OC–HBr	2151	2244	+10	+3

a) Margin of error: 1 cm⁻¹. b) ω B97X-D/aug-cc-pVTZ. c) Bond length: 3.483 Å. d) Bond length: 1.604 Å.

In general, the present result in which we have observed only the long-bond forms is in contrast to our previous work on nitrile–BCl₃ systems, in which only the short-bond forms were observed. In those cases, signals for the long-bond forms may have been obscured due to spectral congestion and CO₂ impurity signals (20, 21). In the present case, we were able to observe the very slight shifts induced by the weak interactions in the long-bond forms of OC–BCl₃ and OC–BBr₃, due to the absence of congestion in the CO region. Normally, one would verify matrix-IR peak assignments via the observation of consistent relative intensities across a range of conditions for a given spectral carrier. That is not possible with the observation of a single peak. For these systems, one might expect to observe fairly strong peaks for the 1:1 complexes in the BX₃ asymmetric stretching region, but with BCl₃ and BBr₃, the occurrence of multiple isotopomers leads to a significant broadening of the free BX₃ signals. This, together with small shifts for the long-bond forms, renders these peaks unobservable. Also, the absence of signals due to the short-bond forms in this region, which would be far-shifted from the free BX₃ signals, is further evidence that these structures are not present to any great extent in our matrix samples.

Conclusion

We have conducted a computational and experimental study of the structural and energetic properties of series of OC–BX₃ complexes. The OC–BF₃ complex has a singular structure with a long, weak B–C bond, and a potential curve reminiscent of systems prone to slight condensed-phase medium effects. In addition, comparisons between previous experimental data and our predicted frequencies are consistent with a slight compression of the B–C bond in an argon matrix environment. Theoretically, OC–BCl₃ is predicted to have two minimum energy structures, so called “short-” and “long-bond” forms, with B–C distances of 1.659 Å and 3.358 Å, respectively; the latter being the global minimum. However, in matrix-IR experiments we were only able to assign peaks to the long-bond form. Much like the BCl₃ complex, OC–BBr₃ also shows the potential for two distinct structures theoretically, with B–C distances of 1.604 Å and 3.408 Å, but the short-bond form is lower in energy according to most methods (CCSD/aug-cc-pVTZ being the notable exception). But again, matrix-IR spectra show evidence for the long-bond form only. Overall, the trends in the features of the B–C potential energy curves can be rationalized by properties of the BX₃ acceptors, and seem to stem from and illustrate a delicate interplay between attractive and repulsive forces along the B–C coordinate.

Conflict of interest statement

There are no conflicts to declare.

Acknowledgments

This work was supported by the National Science Foundation (US) Awards CHE-1566035 and CHE-1626238, as well as the Office of Research and Sponsored Programs at UWEC. This work was made possible via CPU time allotted through the Blugold Supercomputing Cluster (BGSC) at UW–Eau Claire, and via the MERCURY Consortium (supported by National Science Foundation (US) grant #CHE-2018427). Also, J.A.M. and D.T.L. acknowledge support from the WisCAMP program, funded by National Science Foundation (US) Grants #11911284 and #1400815.

Author Contributions

Munos: Investigation, Data Curation, Formal Analysis, Writing – original draft

Lowney: Investigation

Phillips: Conceptualization, Funding Acquisition, Methodology, Project Administration, Supervision, Writing – review and editing

References

1. Rose J. *Molecular complexes*. First edition ed. New York: Pergamon Press: Oxford; 1967.
2. Mulliken RS, Person WB. *Molecular complexes: A lecture and reprint volume*. New York: Wiley-Interscience; 1969.
3. Zhao Y, Truhlar DG. The M06 suite of density functionals for main group thermochemistry, thermochemical kinetics, noncovalent interactions, excited states, and transition elements: two new functionals and systematic testing of four M06-class functionals and 12 other functionals. *Theoretical Chemistry Accounts*. 2008;120(1-3):215-41.
4. Zhao Y, Truhlar DG. Density functionals with broad applicability in chemistry. *Accounts of Chemical Research*. 2008;41(2):157-67.
5. Jonas V, Frenking G, Reetz MT. Comparative Theoretical Study of the Lewis Acid-Base Complexes of BH₃, BF₃, BCl₃, AlCl₃, AND SO₂. *Journal of the American Chemical Society*. 1994;116(19):8741-53.
6. Frenking G, Wichmann K, Fröhlich N, Loschen C, Lein M, Frunzke J, et al. Towards a rigorously defined quantum chemical analysis of the chemical bond in donor-acceptor complexes. *Coordination chemistry reviews*. 2003;238:55-82.
7. Murray JS, Lane P, Clark T, Riley KE, Politzer P. sigma-Holes, pi-holes and electrostatically-driven interactions. *Journal of Molecular Modeling*. 2012;18(2):541-8.
8. Clark T. sigma-Holes. *Wiley Interdisciplinary Reviews-Computational Molecular Science*. 2013;3(1):13-20.
9. Donald KJ, Tawfik M. The Weak Helps the Strong: Sigma-Holes and the Stability of MF₄ center dot Base Complexes. *Journal of Physical Chemistry A*. 2013;117(51):14176-83.
10. Grabowski SJ. π -Hole Bonds: Boron and Aluminum Lewis Acid Centers. *Chemphyschem*. 2015;16(7):1470-9.
11. Phillips JA. Structural and energetic properties of nitrile-BX₃ complexes: substituent effects and their impact on condensed-phase sensitivity. *Theoretical Chemistry Accounts*. 2016;136(1):12.
12. Leopold KR, Canagaratna M, Phillips JA. Partially Bonded Molecules from the Solid State to the Stratosphere. *Accounts of chemical research*. 1997;30(2):57-64.
13. Dvorak MA, Ford RS, Suenram RD, Lovas FJ, Leopold KR. van der Waals vs. covalent bonding: microwave characterization of a structurally intermediate case. *Journal of the American Chemical Society*. 1992;114(1):108-15.
14. Swanson B, Shriver DF, Ibers JA. Nature of the donor-acceptor bond in acetonitrile-boron trihalides. The structures of the boron trifluoride and boron trichloride complexes of acetonitrile. *Inorganic chemistry*. 1969;8(10):2182-9.
15. Burns WA, Leopold KR. UNUSUALLY LARGE GAS-SOLID STRUCTURE DIFFERENCES - A CRYSTALLOGRAPHIC STUDY OF HCN-BF₃. *Journal of the American Chemical Society*.

1993;115(24):11622-3.

16. Phillips JA, Halfen JA, Wrass JP, Knutson CC, Cramer CJ. Large gas-solid structural differences in complexes of haloacetonitriles with boron trifluoride. *Inorganic Chemistry*. 2006;45(2):722-31.
17. Giesen DJ, Phillips JA. Structure, bonding, and vibrational frequencies of $\text{CH}_3\text{CN-BF}_3$: New insight into medium effects and the discrepancy between the experimental and theoretical geometries. *Journal of Physical Chemistry A*. 2003;107(20):4009-18.
18. Buchberger AR, Danforth SJ, Bloomgren KM, Rohde JA, Smith EL, Gardener CCA, et al. Condensed-Phase Effects on the Structural Properties of $\text{FCH}_2\text{CN-BF}_3$ and $\text{ClCH}_2\text{CN-BF}_3$: A Matrix-Isolation and Computational Study. *Journal of Physical Chemistry B*. 2013;117(39):11687-96.
19. Helminiak HM, Knauf RR, Danforth SJ, Phillips JA. Structural and Energetic Properties of Acetonitrile-Group IV (A & B) Halide Complexes. *Journal of Physical Chemistry A*. 2014;118(24):4266-77.
20. Wrass JP, Sadowsky D, Bloomgren KM, Cramer CJ, Phillips JA. Quantum chemical and matrix-IR characterization of $\text{CH}_3\text{CN-BCl}_3$: a complex with two distinct minima along the B-N bond potential. *Physical Chemistry Chemical Physics*. 2014;16(31):16480-91.
21. Phillips JA, Danforth SJ, Hora NJ, Lanska JR, Waller AW. Structural and Energetic Properties of Haloacetonitrile- BCl_3 Complexes: Computations and Matrix-IR Spectroscopy. *Journal of Physical Chemistry A*. 2017;121(48):9252-61.
22. Chatt J, Manojlov.L, Muir KW. X-ray Determination of Molecular Structures of Molybdenum(IV) Oxi-complexes - Possibility of a New Type of Isomerism. *Journal of the Chemical Society D-Chemical Communications*. 1971(13):655.
23. Parkin G. Do Bond-Stretch Isomers Really Exist? *Accounts of Chemical Research*. 1992;25(10):455-60.
24. Pan S, Jana G, Saha R, Zhao LL, Chattaraj PK. Intriguing structural, bonding and reactivity features in some beryllium containing complexes. *Physical Chemistry Chemical Physics*. 2020;22(47).
25. Homray M, Mondal S, Misra A, Chattaraj PK. Bond stretch isomerism in Be-3(2-) driven by the Renner-Teller effect. *Physical Chemistry Chemical Physics*. 2019;21(15):7996-8003.
26. Grabowski SJ. The Nature of TriaI Bonds, a Case of B and Al Centres Bonded with Electron Rich Sites. *Molecules*. 2020;25(11).
27. Feng G, Gou Q, Evangelisti L, Grabow JU, Caminati W. Pulsed jet Fourier transform microwave spectroscopy of the $\text{BF}_3\text{-CO}$ complex. *Journal of Molecular Spectroscopy*. 2017;335:80-3.
28. M. J. Frisch GWT, H. B. Schlegel, G. E. Scuseria, M. A. Robb JRC, G. Scalmani, V. Barone, B. Mennucci, G. A. Petersson HN, M. Caricato, X. Li, H. P. Hratchian, A. F. Izmaylov JB, G. Zheng, J. L. Sonnenberg, M. Hada, M. Ehara KT, R. Fukuda, J. Hasegawa, M. Ishida, T. Nakajima, Y. Honda OK, H. Nakai, T. Vreven, J. A. Montgomery, Jr., et al. Gaussian 09, Revision B.01. Wallingford CT: Gaussian, Inc.; 2010.

29. M. J. Frisch GWT, H. B. Schlegel, G. E. Scuseria, M. A. Robb JRC, G. Scalmani, V. Barone, G. A. Petersson HN, X. Li, M. Caricato, A. V. Marenich, J. Bloino BGJ, R. Gomperts, B. Mennucci, H. P. Hratchian, J. V. Ortiz AFI, J. L. Sonnenberg, D. Williams-Young, F. Ding FL, F. Egidi, J. Goings, B. Peng, A. Petrone, et al. Gaussian 16, Revision C.01. Wallingford CT: Gaussian, Inc.; 2019.
30. Zhao Y, Schultz NE, Truhlar DG. Design of density functionals by combining the method of constraint satisfaction with parametrization for thermochemistry, thermochemical kinetics, and noncovalent interactions. *Journal of Chemical Theory and Computation*. 2006;2(2):364-82.
31. Chai JD, Head-Gordon M. Long-range corrected hybrid density functionals with damped atom-atom dispersion corrections. *Physical Chemistry Chemical Physics*. 2008;10(44):6615-20.
32. Zhao Y, Truhlar DG. Exploring the Limit of Accuracy of the Global Hybrid Meta Density Functional for Main-Group Thermochemistry, Kinetics, and Noncovalent Interactions. *Journal of Chemical Theory and Computation*. 2008;4(11):1849-68.
33. Peverati R, Truhlar DG. Improving the Accuracy of Hybrid Meta-GGA Density Functionals by Range Separation. *Journal of Physical Chemistry Letters*. 2011;2(21):2810-7.
34. Peverati R, Truhlar DG. Screened-exchange density functionals with broad accuracy for chemistry and solid-state physics. *Physical Chemistry Chemical Physics*. 2012;14(47):16187-91.
35. Cramer CJ. *Essentials of computational chemistry: theories and models*: Wiley. com; 2005.
36. Herzberg G. *Molecular spectra and molecular structure*. Second edition. ed. Malabar, Fla.: Malabar, Fla. : R.E. Krieger Pub. Co.; 1989.
37. Waller AW, Weiss NM, Decato DA, Phillips JA. Structural and energetic properties of haloacetonitrile – GeF₄ complexes. *Journal of Molecular Structure*. 2017;1130:984-93.
38. Wells NP, Phillips JA. Infrared spectrum of CH₃CN-BF₃ in solid argon. *Journal of Physical Chemistry A*. 2002;106(8):1518-23.
39. Eigner AA, Rohde JA, Knutson CC, Phillips JA. IR spectrum of CH₃CN-BF₃ in solid neon: Matrix effects on the structure of a Lewis acid-base complex. *Journal of Physical Chemistry B*. 2007;111(6):1402-7.
40. Mantina M, Chamberlin AC, Valero R, Cramer CJ, Truhlar DG. Consistent van der Waals Radii for the Whole Main Group. *Journal of Physical Chemistry A*. 2009;113(19):5806-12.
41. Cordero B, Gomez V, Platero-Prats AE, Reves M, Echeverria J, Cremades E, et al. Covalent radii revisited. *Dalton Transactions*. 2008(21):2832-8.
42. Phillips JA, Cramer CJ. Quantum chemical characterization of the structural and energetic properties of HCN-BF₃. *Journal of Chemical Theory and Computation*. 2005;1(5):827-33.
43. Smith EL, Sadowsky D, Phillips JA, Cramer CJ, Giesen DJ. A Short Yet Very Weak Dative Bond: Structure, Bonding, and Energetic Properties of N₂-BH₃. *The journal of physical chemistry A, Molecules, spectroscopy, kinetics, environment, & general theory*. 2010;114(7):2628-36.
44. Brinck T, Murray JS, Politzer P. *Computational Analysis of the Bonding in Boron-Trifluoride and Boron-Trichloride and Their Complexes with Ammonia*. *Inorganic Chemistry*.

1993;32(12):2622-5.

45. Smith EL, Sadowsky D, Cramer CJ, Phillips JA. Structure, Bonding, and Energetic Properties of Nitrile-Borane Complexes: RCN-BH₃. *Journal of Physical Chemistry A*. 2011;115(10):1955-63.
46. Gebicki J, Liang J. IR evidence for the formation of weakly bound complexes BF₃-CO and BF₃-N₂. *Journal of molecular structure*. 1984;117(3-4):283-6.
47. Nxumalo LM, Ford TA. The boron trifluoride-carbon monoxide complex: A matrix-isolation infrared spectroscopic and ab initio molecular-orbital theoretical study. *South African journal of chemistry*. 1995;48(1-2):30-8.